Fractal Shaped Periodic Metal Nanostructures Atop Dielectric-Metal Substrates for SERS Applications

Novikov, Sergey M.; Boroviks, Sergejs; Evlyukhin, Andrey B.; Tatarkin, Dmitry E.; Arsenin, Aleksey V.; Volkov, Valentyn S.; Bozhevolnyi, Sergey I.

Published in:
ACS Photonics

DOI:
10.1021/acsphotonics.0c00257

Publication date:
2020

Document version:
Accepted manuscript

Citation for pulished version (APA):
Novikov, S. M., Boroviks, S., Evlyukhin, A. B., Tatarkin, D. E., Arsenin, A. V., Volkov, V. S., & Bozhevolnyi, S. I. (2020). Fractal Shaped Periodic Metal Nanostructures Atop Dielectric-Metal Substrates for SERS Applications. *ACS Photonics*, *7*(7), 1708-1715. https://doi.org/10.1021/acsphotonics.0c00257

Article

Fractal shaped periodic metal nanostructures atop dielectric-metal substrates for SERS applications

Sergey M. Novikov, Sergejs Boroviks, Andrey B. Evlyukhin, Dmitry E. Tatarkin, Aleksey V Arsenin, Valentyn S. Volkov, and Sergey I. Bozhevolnyi

ACS Photonics, **Just Accepted Manuscript** • DOI: 10.1021/acsphotonics.0c00257 • Publication Date (Web): 16 Jun 2020

Fractal shaped periodic metal nanostructures atop dielectric-metal substrates for SERS applications

Sergey M. Novikov, [*, †, ‡] *Sergejs Boroviks,* [‡] *Andrey B. Evlyukhin,* [†, &] *Dmitry E. Tatarkin,* [†] *Aleksey V. Arsenin,* [†] *Valentyn S. Volkov,* [†,] *Sergey I. Bozhevolnyi* [‡,§]

[†]Center for Photonics and 2D Materials, Moscow Institute of Physics and Technology, 9 Institutsky Lane, 141700, Dolgoprudny, Russia.

[‡] Centre for Nano Optics, University of Southern Denmark, Campusvej 55, DK-5230 Odense, Denmark.

[§]Danish Institute for Advanced Study, University of Southern Denmark, Campusvej 55, DK-5230 Odense M, Denmark

[&] Institute of Quantum Optics, Leibniz Universität Hannover, Welfengarten str.1, 30167 Hannover, Germany.

[*]Corresponding author's email: novikov.s@mipt.ru

ABSTRACT: Controlled and reliable field enhancement (FE) effects associated with the excitation of plasmons in resonant metal nanostructures constitute an essential prerequisite for the development of various sensing configurations, especially those utilizing surface-enhanced Raman scattering (SERS) spectroscopy techniques. Leveraging advantages of random nanostructures in providing strong collective resonances in a broad wavelength range with the design flexibility of individual gap plasmon resonators, we experimentally investigate fractal shaped arrays of gap plasmon resonators and characterize the occurring FE effects by mapping SERS signals from uniformly spread Rhodamine 6G with high-resolution Raman microscopy. In such geometry, the total FE is expected to benefit from both FE associated with gap plasmon excitation and FE due to constructive interference of the surface plasmon modes reflected and diffracted by fractal shaped boundaries. Linear reflection imaging spectroscopy is used to verify that the fabricated nanostructures exhibit spatially distributed resonances (bright spots) close to the excitation wavelengths used for the Raman microscopy. The positions of bright spots are argued to be influenced by fractal shaped boundaries, particle dimensions, polarization, and wavelength of the incident and scattered light. Experimentally obtained SERS images from similar fractal (gold) structures fabricated with different dielectric SiO_2 spacer thicknesses (0, 20 and 40 nm) featured diffraction-limited bright spots corresponding to local SERS enhancements of up to ~ 10^7 (relative to Raman signals obtained with a glass substrate) for 40-nm-thick SiO_2 layers. Our results indicate that the strategy of combining fractal array geometry with gap plasmon resonances is promising for the design of highly efficient SERS substrates for potential applications in surface-enhanced multichannel sensing, including single-molecule spectroscopy.

KEYWORDS: plasmonics, field enhancement, SERS, scanning microscopy, fractals, linear and nonlinear light scattering by nanostructures, gap surface plasmons.

Introduction

Surface-enhanced Raman scattering (SERS) spectroscopy is a highly selective and non-destructive optical tool for chemical identification of molecular composition with very low, on the order of nM, concentrations of target molecules.[1] First observed as a scattering phenomenon in 1974,[2] SERS has been rapidly developing into a powerful spectroscopic characterization technique widely exploited in the ever-expanding range of applications ranging from biomolecular sensing, biochemistry and medical diagnostics to material and environmental science.[1-5] Recently, even the single-molecule detection of contaminants, explosives, and viruses was shown to be possible.[6-9]

The main physical mechanism behind SERS is related to strong electromagnetic field enhancement (FE),[10] which occurs due to resonant excitations of surface plasmons (SPs), i.e., collective electron excitations in metals coupled to electromagnetic fields in dielectrics.[11-13] In general, two types of resonant excitations can be distinguished: localized SP excitations in nanostructures of different shapes and compositions and propagating SP modes supported by metal-dielectric interfaces commonly referred to as surface plasmon polaritons (SPPs). The spectral positions of resonances can be tuned by changing the geometry (shape and size) of nanostructures, their constitutive materials, and the refractive index of the surrounding medium.[1] Judiciously engineered plasmonic nanostructures allow thereby for the realization of strong FE effects in different wavelength ranges.[14-16]

Various strategies have been suggested in order to realize strong and robust FE effects for applications in SERS.[17-22] From the applicational viewpoint, the design of highly efficient SERS substrates represents one of the most active research directions, motivating investigations of SERS enhancements that can be achieved in ensembles of surface nanostructures with

sufficiently high surface coverage.[1,23] Large-scale realistic simulations of nanoparticle-based SERS substrates indicate, while the SERS enhancement generally increases with the coverage, very large individual FEs are not necessarily improve the SERS enhancement of close-packed arrays.[23] Among plasmonic configurations ensuring relatively large and robust FE effects, metal nanostructures separated by subwavelength-thin dielectric spacers from metal substrates, which support highly confined plasmonic modes known as gap SPs (GSPs), are attractive because their resonances are easily tuned by geometry and associated with the excitation of magnetic-dipole current configurations with strongly suppressed radiative damping.[24] The underlying mechanism of GSP resonators is similar to that of a Fabry-Perot resonator with the resonance occurring due to constructive interference of GSP modes reflected at the resonator terminations.[24-27] The GSP resonance characteristics can be controlled by modifying the spatial extent of the top nanostructures, material, and thickness of the dielectric spacer gap width, with the possibility of reaching extreme FEs for ultrathin gaps.[28]

Considering approaches to cover large substrate areas with nanostructures, the usage of fractal patterns in the geometry of plasmonic nanostructures is appealing because these structures are known to support multiple tunable resonances over broad spectral domains.[29,230] Generally, these resonances are associated with the formation of subwavelength-localized areas with strong FEs, so-called hot spots, in the regions of constructive interference of corresponding (localized and/or propagating SP) modes.[29] Fractal structures featuring various FE effects have found diverse applications,[30] ranging from subwavelength imaging,[31] broadband absorbers,[32] sensors,[33] to graphene photodetectors.[34] We have previously explored light scattering by fractal shaped periodic arrays of gold nanoparticles fabricated on thick gold films, and associated generation of localized FEs.[35, 36] The boundary of such structure is defined by the shape of the Mandelbrot

fractal,[37] and hot spots are produced inside the structure due to the interference of (excited by scattering of incident radiation) SPP waves that are reflected and diffracted at the boundaries.[35,38] The underlying physical mechanism of hot spot generation[35] is therefore similar to the mode formation in acoustic fractal drums.[39] Extensive optical characterization of FE effects in these nanostructured arrays demonstrated that the possibility of reproducibly realizing an order of magnitude gain in SERS signal with respect to that measured with unstructured gold films. [40-2]

In this work, we take advantage of the aforementioned attractive features of individual GSP resonators, including efficient SPP excitation by GSP scattering,[26] by arranging cylindrical gold nanoparticles in a periodic array shaped by the Mandelbrot fractal[35] atop a thick gold film covered by a thin SiO_2 spacer layer of different thicknesses (0, 20 and 40 nm). We use scanning confocal Raman microscopes operating at the wavelengths of 532 and 632.8 nm to map SERS signals from Rhodamine 6G (R6G) homogenously adsorbed on the fabricated samples. Linear reflection imaging spectroscopy is used to verify that the fabricated nanostructures exhibit spatially distributed resonances (bright spots) close to the excitation wavelengths used for the Raman microscopy. The positions of bright spots are argued to be influenced by fractal shaped boundaries, particle dimensions, polarization and wavelength of the incident and scattered light. The SERS images from all fractal structures feature diffraction-limited hot spots corresponding to local SERS enhancements of up to ~27 and ~55 (relative to the fractal on the bare gold film) for 20- and 40-nm-thick SiO_2 spacer layers, respectively, with overall SERS enhancements of up to ~ 10^7 relative to Raman signals obtained with a glass substrate. Our results demonstrate that fractal shaped arrays of GSP resonators are promising for the design of highly efficient SERS substrates for potential applications in surface-enhanced multichannel sensing, including single-molecule spectroscopy.

RESULTS AND DISCUSSION

Linear and optical characterization. We fabricate 180-nm-period square arrays of cylindrical (height of 50 nm, diameter of 100 nm) gold nanoparticles (NPs) formed on a continuous smooth optically thick (120 nm) gold film (Figure 1a) and atop dielectric-metal substrates consisting of a similar thick gold film and SiO_2 layers (Figure 1b,c, Figure S1) using electron beam lithography (EBL). The boundaries of the arrays are defined by the shape of a segment of the Mandelbrot fractal. The thicknesses of dielectric layers are 20 nm and 40 nm. For more details on the fabrication, see the Methods section. The scanning electron microscope (SEM) images (Figure 1d-f) of a fractal with SiO_2 thickness 40 nm demonstrate the high quality and no visible defects of the fabricated samples. Before SERS investigations, the fabricated samples were characterized by optical microscopy with white-light illumination and linear reflection imaging spectroscopy (see Methods).

The optical white-light images of fractals obtained in co- and cross-polarizations with GSP resonator and NP arrays and demonstrate distinctly different features. The fractal structure formed on the bare gold film viewed with the co-polarized illumination produces a dark-shaded fractal structure, although with a very low optical contrast with (Figures S2a,d) due to weak NP resonances in the visible, most pronounced near 540 nm (Figure 1b). Similar fractal structures representing GSP resonators generate strong green colors (Figure 2a and S2b,c,e,f) due to strong absorption in the red part of the spectrum (Figure 2b) caused by the GSP resonances at these wavelengths.[43,44] The optical images of NP and GSP fractals obtained with the cross-polarized illumination, which can be considered as scattering images, show consequently weakly contrasted

greenish (Figure S2g) and bright red-colored images with very intense hot spots (Figure 2c and Figure S2h,i).

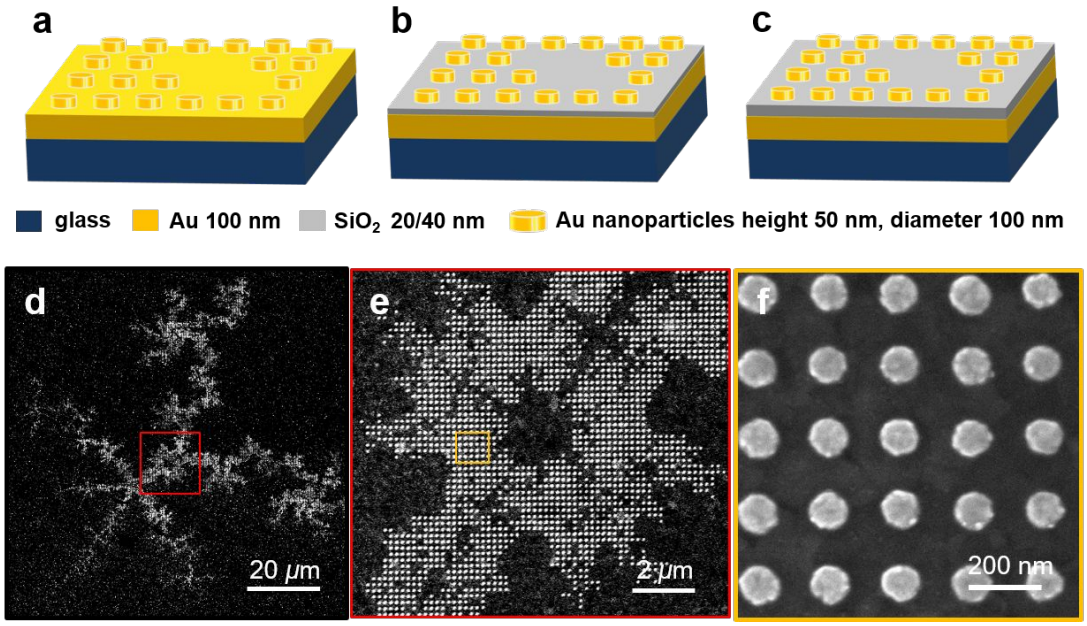

Figure 1. Schematic images of fractal structure a) on the bare gold film b) on the gold film with a layer of SiO_2 20 nm c) on the gold film with a layer of SiO_2 40 nm; d)-f) SEM images of a fractal with the thickness of SiO_2 40 nm.

The sample characterization with the linear reflection imaging spectroscopy resulted in the spectrally resolved high-resolution images (see Methods) of each sample obtained with the co- and cross-polarized illuminations (Figure S3-S5). The reflection spectra obtained with the co-polarized illumination for all fractal samples indicate the presence of two (although differently pronounced) resonances, at ~550 and ~650-670 nm (Figure 2b). The short-wavelength resonance, practically disappearing for large spacer thickness (being transformed in progressively weaker shoulders in the resonance curves), is apparently associated with the excitation of individual NP resonances, i.e., practically without the influence of the gold substrate in case of GSP fractals.[445] The long-

wavelength resonance, very weakly pronounced for the NP fractal configuration, is ascribed to the occurrence of constructive interference of SPP or GSP waves excited by scattering of the incident light by nanostructures and reflected/diffracted by fractal shaped boundaries.

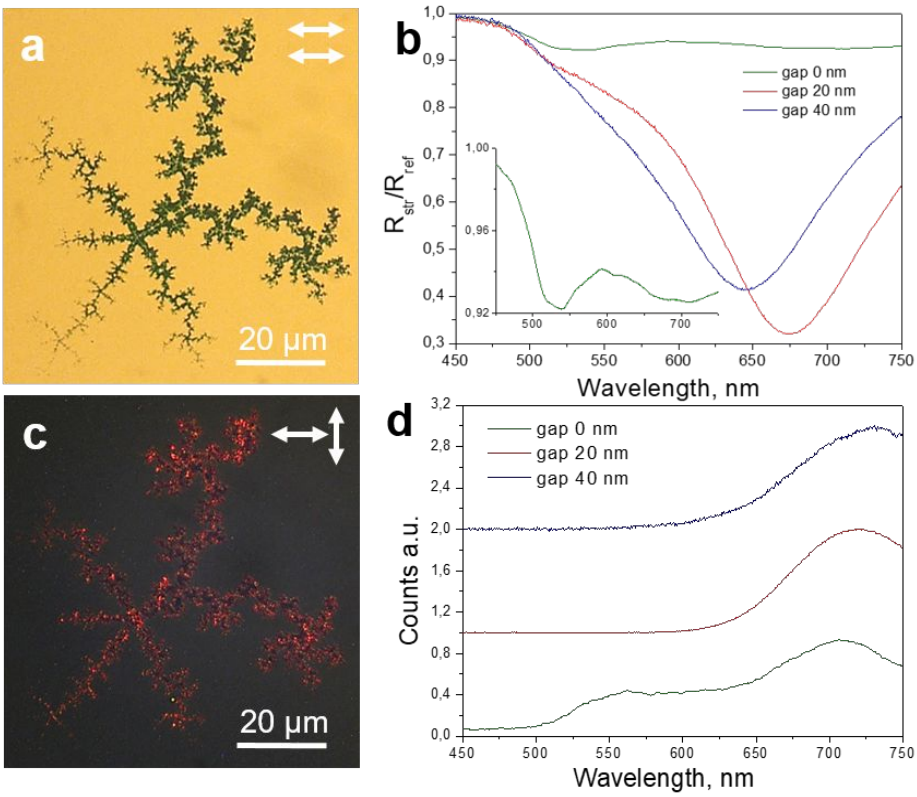

Figure 2. Optical images of the fractal structure fabricated on a substrate with a 40 nm SiO_2 gap obtained in a) co-polarized and c) cross-polarized detection and illumination; b) reflection and d) scattering spectra from typical hot spots in fractal images for various spacer thicknesses.

The collective resonance for the NP fractal configuration is very weak because the NP scattering efficiency of SPP excitation along with the SPP reflection by the fractal boundaries is small due to a relatively low NP height (and thereby volume).[35] The corresponding weak reflection minimum (inset in Figure 2b) is a result of competing trends: SPP absorption at shorter (< 600 nm)

wavelength (that jeopardizes the SPP multiple scattering) and a rapidly decreasing with the wavelength NP scattering efficiency. The GSP excitation and scattering (and reflection by the fractal boundaries) are expected to significantly (in comparison) increase due to strong individual GSP resonances (as discussed above) and efficient excitation of SPP waves by GSP resonators.[26] The GSP resonances become stronger and red-shifter for smaller spacer thicknesses,[44] resulting in a deeper and red-shifted minimum in the reflection spectrum for the 20-nm-thick spacer as compared to that for the 40-nm-thick one (Figure 2b). Essentially, smaller spacer thicknesses result in shorter GSP wavelengths (i.e., larger GSP effective indexes) and, consequently, stronger reflections at the resonator terminations and larger resonance (vacuum) wavelengths.[27] Note that, in this case, the same competing trends as above result in the trade-off being very close to the resonant wavelength of the constituent individual GSP resonators, enhancing thereby their effect as compared to the reflection minima observed for the individual GSP resonators.[43,44]

Spectrally-resolved fractal images obtained with the co-polarized illumination appear relatively homogeneous (Figure S2a-c), whereas the corresponding images with the cross-polarized illumination display a set of bright spots (Figure S3d-f), whose position and number correlates (not surprisingly) with the white-light bright fractal images obtained with the cross-polarized illumination (Figure S2g-i). At the same time, the fractal nature of GSP resonator array boundaries results in irregular multiple scattering and interference leading to different position-dependent scattering spectra, i.e., spectra obtained by spectrally-resolved microscopy from different regions with the cross-polarized illumination (Figure 2d and Figure S4). These noticeable differences confirm the collective nature of the observed resonances, since multiple GSP scattering, reflection by fractal boundaries and interference are expected to be noticeably influenced by the local (within the GSP propagation length) fractal shape.

Raman characterization. Characterization of the FE effects in fractal structures was conducted using the Raman microscopy (see Methods) with all samples being covered by an aqueous 10^{-6} M solution of R6G for approximately 1 h and subsequently gently blown dry with compressed air. Typical SERS images obtained with all fractal structures replicate clearly the fractal geometry defined by the EBL, while also revealing several hot spots (Figure 3a-c).

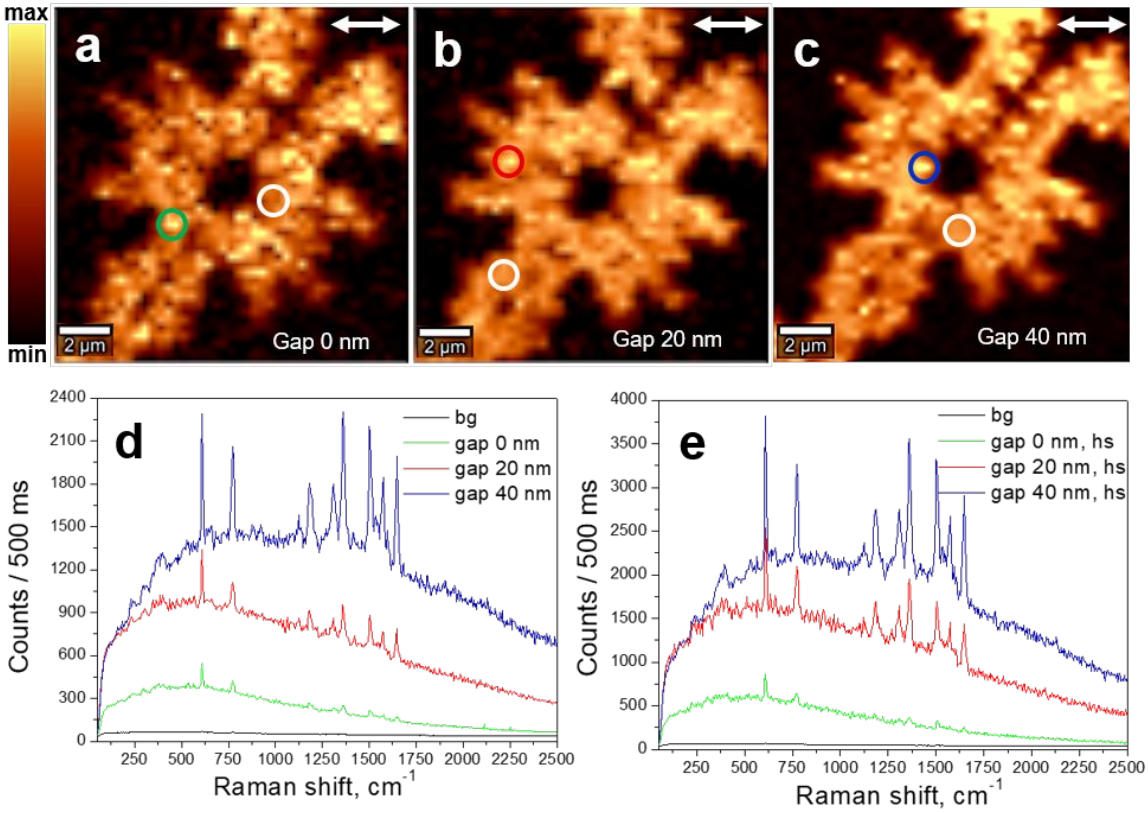

Figure 3. a, b, c) Raman images obtained with the illumination at the wavelength of 532 nm by mapping Raman signals integrated over 1465–1620 cm^{-1} from R6G adsorbed on fractal NPs with a) gap 0 nm, b) gap 20 nm, c) gap 40 nm d) Typical Raman spectra recorded from the points outside hot spots, marked with white rings. e) Raman spectra of selected hot spots marked as green, red, and blue rings on the a-c). Reference spectra (bg - in the legend) were obtained from the bare gold film.

Based on our previous investigations involving both two-photon luminescence microscopy,[35,38] and SERS, [40] we attribute hot spots to the occurrence of constructive interference of SPPs (in the case of gold NPs fabricated on a bare gold film) and GSPs (in the case of gold NPs fabricated on a SiO_2 spacer supported by the gold film), which are excited by the incident radiation (due to the scattering by NPs) and partially reflected by fractal shaped boundaries.

Raman spectra demonstrate that the intensity of Raman peaks is dramatically enhanced by using the GSP fractal configurations in comparison with the NP structures fabricated on the bare gold film metal, with the strongest enhancement achieved with the 40-nm-thick SiO_2 spacer (Figure 3d,e). The observed difference in SERS signals obtained with GSP resonators and those with NP structures is a result of stronger interaction of incident radiation with GSP resonators and more efficient excitation of SP modes. This substantially changes the resonance excitation condition in the system and adds an additional degree of freedom for their control by controlling the gap thickness. The difference in the observed SERS enhancements for different fractal configurations is consistent with the features of optical resonances observed in the corresponding reflection spectra (Figure 2b). We believe that the Raman signals obtained with the 40-nm-thick SiO_2 spacer are additionally enhanced due to the relative (to the 20-nm-thick SiO_2 spacer) increase in the scattering and decrease in the absorption of the GSP resonators[46] that facilitate emission (re-radiation) of Raman-shifted photons.[1] The Raman signals obtained from the hot spots (Figure 3e) have the strengths of up to 3 times higher in comparison with those collected from the places outside the hot spots (Figure 3d). Importantly, the hotspot positions are determined by the configuration of fractal structures, the dielectric gap, and resonant field frequency. The occurrence

of SERS hotspots is a reproducible feature of this system and, therefore, can be used for the development of improved SERS structures and their potential applications.

A similar trend was observed with the SERS spectra obtained with the excitation laser operating at the wavelength of 632.8 nm (Figure S4), although the difference between the SERS signals from the GSP fractals and those from the NP fractal became significantly larger (cf. Figure 3d,e and Figure S7a,b). This difference increase matches well the increase in the difference between the corresponding reflection spectra when comparing the pump wavelengths of 532 and 632.8 nm (Figure 2b). It should, however, be noted that the above comparison is conducted for the SERS signals that also include the background fluorescence contribution, which is primarily driven by the absorption of the pump illumination that also determines the reflection spectra. Raman scattering and fluorescence are two competing phenomena, and the laser-induced fluorescence is a source of omnipresent background signals. If the metal surface is rough or nanostructured, the intensity of fluorescence can also be enhanced, a phenomenon that is termed surface-enhanced fluorescence. This phenomenon is also observed in the experiments with our structures. The fluorescence background is stronger for GSP configurations than that for NP structures, a tendency that is similar to that observed for SERS signals. In order to quantify the benefit of using GSP-based configurations with respect to the SERS signals appearing on the top of the fluorescence, we carefully subtracted the average fluorescence background and compared levels of six main R6G Raman peaks normalizing their signals by those obtained with the NP (zero-spacer-thickness) fractal configuration (Figure 4). The corresponding SERS enhancements (relative to the NP fractal configuration) are up to ~11 and ~37 (with the 532-nm-wavelength pump) and ~27 and ~55 (with the 632.8-nm-wavelength pump) for the GSP fractal configurations with the 20- and 40-nm-thick SiO_2 spacers, respectively. It is thereby seen that also the pure SERS signal enhancements follow

the differences in the reflection spectra for these wavelengths (Figure 2b). These features are also consistent with the conclusions of the previous experimental investigations using scanning two-photon photoluminescence microscopy that GSP resonator arrays significantly enhance local electric fields.[27]

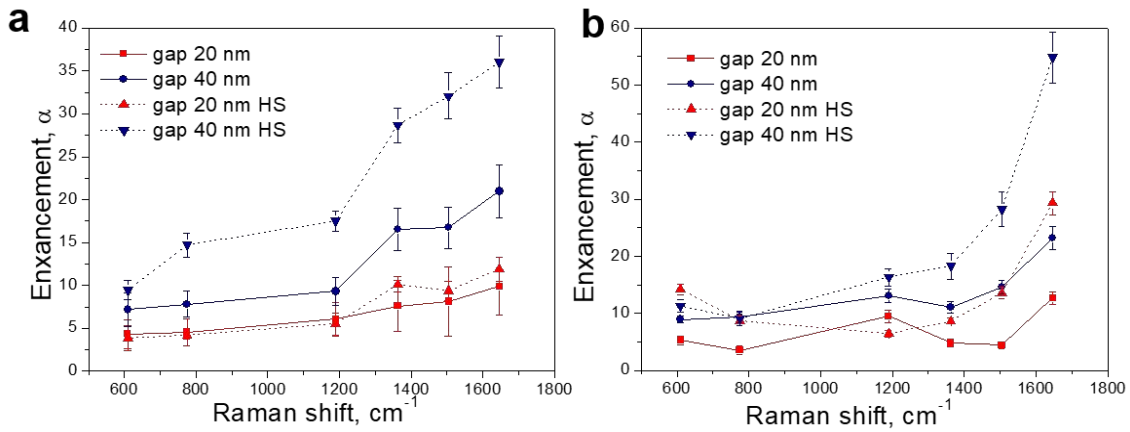

Figure 4. Relative Raman enhancement estimated as the relation between intensity obtained from metal nanostructures atop dielectric-metal substrates and intensity obtained from the fractal on the bare gold film with a) wavelength 532 nm, b) wavelength 632.8 nm. HS - hot spots**.**

The analysis of Raman images recorded by counting Raman signals from different spectral regions of R6G Raman signals (for instance, 610–625 cm^{-1} and 1465–1620 cm^{-1}), allows one to observe the associated variations in the strength of some hot spots (Figure S8). A number of the bright spots change their mutual strength, while some appear only in one of the images (e.g., spots 1 and 2 indicated by white circles in Figure S8). At the same time, the data used for the generation of both these images were recorded simultaneously, making up the same set of spatially-resolved Raman spectra. The fact, that these two images (Figure S8) generated by selecting different peaks in the spectra (i.e., at 610–625 cm^{-1} and 1465-1620 cm^{-1} corresponding to the wavelengths of ~552 and ~583 nm, respectively, when using the 532-nm-wavelength pump) are not identical,

indicates that the local field enhancements determining SERS signals have spatially different spectra, as also seen directly from the scattering spectra obtained at different locations (Figure S6). We will not go into a detailed discussion of these issues since there is a number of publications specifically devoted to this matter.[47-49] The previously formulated conclusion that the differences in scattering spectra confirm the collective nature of the observed resonances, i.e., their origin in multiple GSP scattering, reflection by fractal boundaries and interference, can thereby be also supported with the discussed Raman images and signals (Figure S8). It should also be borne in mind that the local FE at other spatial positions might be at resonance outside the wavelength range probed via mapping the R6G Raman signals, implying that the maximum SERS enhancements achievable with these configurations can be even higher. Finally, we would like to emphasize that the hot spots observed in the Raman images do not originate from uneven distributions of R6G pigment or fabrication defects. In order to support this conjecture, we fabricated square-shaped arrays (see Methods) with the parameters used in the fractal-shaped structures and conducted SERS microscopy imaging of these arrays. The SERS images obtained with the square-shaped arrays exhibit rather homogeneous signal distributions without hotspots (Figure S7). These observations confirm our supposition that the presence of hotspots in SERS images of fractal structures is not associated with the effect of uneven deposition of dye molecules.

Furthermore, the comparison of high-resolution SEM images of the fractal structures and their SERS images demonstrates a very good correlation without any apparent defects (Figure S10).

To compare the signal increase in SERS with that in ordinary Raman while keeping the same experimental parameters, the analytical enhancement factor (EF expression) is used.[50] The average EF is determined by comparing the signals acquired from R6G at a concentration of 10^{-2}

M on a glass substrate, with the signals obtained from 10^{-6} M of R6G on the fractal structures on the metal and on the MIM structures. The following equation is used:

$$EF = \frac{I_{SERS}\, C_{REF}}{I_{REF}\, C_{SERS}} \qquad 1$$

Where the I_{SERS} and I_{REF} correspond to background-subtracted intensities of R6G adsorbed on the fractal structures and the glass substrate, respectively. C_{SERS} and C_{ref} represent the corresponding concentrations of R6G on these structures. The average EF values are estimated to be ~0.25×10^6 (for the fractal on the bare gold film), ~0.28×10^7 (for the fractal on the 20-nm-thick SiO_2 spacer) and ~0.93×10^7 (for the fractal on the 40-nm-thick SiO_2 spacer) in the case of the laser 532 nm respectively. In the case of using of the laser 632.8 nm the EF values are estimated to be ~0.17×10^6 (for the fractal on the bare gold film), ~0.44×10^7 (for the fractal on the 20-nm-thick SiO_2 spacer) and ~0.83×10^7 (for the fractal on the 40-nm-thick SiO_2 spacer) respectively. We should stress the hot spots can be damaged by local heating and the R6G is easy to destroy, and during the scanning, it was necessary to find a compromise between the signal and good resolution, that is why the real enhancement estimation would be 1 or even 2 orders of magnitude higher.

CONCLUSIONS

To summarize, we use Raman microscopy to map SERS from R6G with a concentration of 10^{-6} M uniformly spread on the cylindrical gold nanoparticles in a periodic array (shaped by the Mandelbrot fractal) atop a thick gold film covered by a thin SiO_2 spacer layer of different thicknesses (0, 20 and 40 nm). In order to estimate the benefit of using GSP-based

configurations, we compared levels of the six main R6G Raman peaks. The SERS images from fabricated samples featured diffraction-limited bright spots corresponding to local SERS enhancements of up to ~27 and ~55 (relative to the fractal on the bare gold film) for 20- and 40-nm-thick SiO_2 spacer layers, respectively. Overall SERS enhancement factor, relative to Raman signals obtained with a glass substrate, was estimated to be up to ~ 10^7. The position of bright spots is dependent on the fractal shaped boundaries, particle dimensions, polarization, and wavelength of the incident and scattered light. Linear reflection spectroscopy was used to verify that nanostructures exhibit resonances close to excitation wavelengths used for the Raman microscopy. The obtained results demonstrate that the combination of two complementary design strategies for field enhancement in SERS substrates - GSP resonators and fractal-shaped array boundaries is a perspective approach for the development of SERS substrates for surface-enhanced multichannel sensing, e.g., SERS based diagnostics, single-molecule spectroscopy and other kinds of bio-molecule optical sensing.

METHODS

Fabrication. The samples were fabricated using standard EBL and lift-off techniques. First, the substrates were prepared: 2 nm of Ti and 120 nm of Au and another 2 nm layer of Ti were deposited in a Cryofox 600 Explorer chamber using thermal evaporation at rates 0.01 nm/s for Ti and 0.1 nm/s for Au respectively. Thin titanium layers were introduced as they promote adhesion of the gold to the silicon wafer and adhesion of subsequently deposited SiO_2 to the gold layer. After that, the wafer was cut into smaller chips of sizes ~1×1 cm^2. Further, several chips were covered with ~20 nm layer of SiO_2, another part of chips with ~40 nm and the remaining chips were left intact. SiO_2 deposition was performed in the same chamber, but using radio-frequency

sputtering of SiO_2 target at 200 W power. Hereafter 100 nm of e-beam resist - polymethyl methacrylate (PMMA) (950k A2, purchased from Microchem) - was spin-coated onto the wafer at 500 RPM for 5 s and 1600 RPM for 45 s and subsequently baked on a hot plate at 180 °C for 120 s. Locations of nanoparticles in the fractal pattern were calculated to form an array with 180 nm period, which fills the inner region of a small branch of the Mandelbrot fractal[35] extending over ~ 100×100 μm^2. The pattern was exposed as dots using the ELPHY EBL Quantum system attached to a JEOL JSM6490 SEM. Additionally, the square-shaped 15×15 μm^2 arrays with the same periodicity were patterned. After the exposure and development using diluted methyl isobutyl ketone (MIBK) solvent, another stack of 2 nm Ti and 50 nm Au was deposited. After the exposure and development using diluted methyl isobutyl ketone (MIBK) solvent, another stack of 2 nm Ti and 50 nm Au were deposited. Finally, the lift-off procedure was performed: the sacrificial PMMA layer was etched in acetone overnight, and the samples were subsequently cleaned with isopropanol.

SEM. We used a JEOL JSM6490 and JEOL JSM-7001F scanning electron microscopes (SEM) for the characterization of samples.

Optical characterization. Optical images were acquired using a Zeiss Observer microscope (EpiplanNeofluar HD objective ×100, NA=0.90). Linear polarizer and analyzer were used to select appropriate polarization of the illumination and detected light. A standard tungsten-halogen lamp was used as illumination. The spectroscopic reflection analysis was performed using the Andor's Kymera 193i spectrograph equipped with the Andor's Newton CCD camera. The width of the slit of the spectrometer was adjusted so that the image area analyzed by the spectrometer is ~2×80 μm. The spectral portrait of each sample was obtained by scanning across

the structures with a step of 2 μm. Reported spectra were normalized to a reference spectrum, obtained outside fractals in the same conditions.

Raman microscopy. The experimental setups used for Raman microscopy are: 1) The commercially available confocal scanning Raman microscope (Alpha300R, Witec). The measurements were obtained using linearly polarized excitation of wavelength 532 nm, 600 lines/mm diffraction grating, and ×100 objective (N.A. = 0.90). 2) The confocal scanning Raman microscope Horiba LabRAM HR Evolution. The measurements were obtained using linearly polarized excitation of wavelength 632.8 nm, 300 lines/mm diffraction grating, and ×100 objective (N.A. = 0.90). We use unpolarized detection in order to have a significant signal to noise ratio. Detailed SERS images were formed by mapping the spatial dependence of SERS intensity integrated around the main Raman peaks within the shift range 1560-1650 cm^{-1} for each of the 28 × 28 points (step size 350 nm) in the scan, incident powers P~ 0.08 mW and an integration time of 500 ms at each point.

ASSOCIATED CONTENT

Supporting Information. Additional figures with results of the characterization of the fractal shaped structures.

AUTHOR INFORMATION

Corresponding Author

*E-mail: novikov.s@mipt.ru

Author Contributions

S. I. B. conceived the experiment. S. B. designed and fabricated the samples. S. B. and S.M.N. performed the electron microscopy (SEM). S. M. N. and D.E.T performed the Raman

measurements, V. S. V. and A. B. E. conducted optical spectroscopy. S. M. N., S. B. and A.V. A. drafted the manuscript. All authors discussed the results and commented on the manuscript. S. I. B. supervised the project.

Notes

The authors declare no competing financial interests

ACKNOWLEDGMENT

Analysis of the optical resonances and spectroscopic results has been supported by the Russian Science Foundation Grant No. 20-12-00343. S.B. is supported by VILLUM FONDEN (grant No. 16498). S.I.B. acknowledges the European Research Council, Grant 341054 (PLAQNAP). Center for Nano Optics is financially supported by the University of Southern Denmark (SDU 2020 funding). We thank the Shared Facilities Center of the Moscow Institute of Physics and Technology (grant no. RFMEFI59417X0014) for the use of their equipment. Part of the authors acknowledges financial support from the Deutsche Forschungsgemeinschaft (DFG, German Research Foundation) under Germany's Excellence Strategy within the Cluster of Excellence PhoenixD (EXC 2122, Project No. 390833453). We acknowledge A.S. Roberts and F. Todisco for efforts in assembling the optical characterization setup.

REFERENCES

(1) Langer, J.; Jimenez de Aberasturi, D.; Aizpurua, J.; AlvarezPuebla, R. A.; Auguie, B.; Baumberg, J. J.; Bazan, G. C.; Bell, S. E. J.; Boisen, A.; Brolo, A. G.; Choo, J.; Cialla-May, D.; Deckert, V.; Fabris, L.; Faulds, K.; García de Abajo, F. J.; Goodacre, R.; Graham, D.; Haes, A.

J.; Haynes, C. L.; et al. Present and Future of Surface-Enhanced Raman Scattering. *ACS Nano* **2020**, *14*, 28-117.

(2) Fleischmann, M.; Hendra, P.; McQuillan, A. Raman spectra of pyridine adsorbed at a silver electrode. *Chem. Phys. Lett.* **1974**, *26,* 163 - 166.

(3) Gruenke, N. L.; Cardinal, M. F.; McAnally, M. O.; Frontiera, R. R.; Schatz, G. C.; Van Duyne, R. P. Ultrafast and nonlinear surface-enhanced Raman spectroscopy. *Chem. Soc. Rev*. **2016**, *45*, 2263–2290.

(4) Kneipp, K.; Moskovits, M.; Kneipp, H. *Surface-Enhanced Raman Scattering: Physics and Applications;* Topics in Applied Physics; Springer Berlin Heidelberg, 2006.

(5) McNay, G.; Eustace, D.; Smith, W. E.; Faulds, K.; Graham, D. Surface-Enhanced Raman Scattering (SERS) and Surface-Enhanced Resonance Raman Scattering (SERRS): A Review of Applications. *Applied Spectroscopy* **2011**, *65*, 825–837, PMID: 21819771.

(6) Kneipp, K.; Wang, Y.; Kneipp, H.; Perelman, L. T.; Itzkan, I.; Dasari, R. R.; Feld, M. S. Single Molecule Detection Using Surface-Enhanced Raman Scattering (SERS). *Phys. Rev. Lett.* **1997**, *78*, 1667–1670.

(7) Yang, S.; Dai, X.; Stogin, B. B.; Wong, T.-S. Ultrasensitive surface-enhanced Raman scattering detection in common fluids. *Proceedings of the National Academy of Sciences* **2016**, *113*, 268–273.

(8) Etchegoin, P. G.; Le Ru, E. C. A perspective on single molecule SERS: current status and future challenges. *Phys. Chem. Phys*. **2008**, *10*, 6079–6089.

(9) Kneipp, J.; Kneipp, H.; Kneipp, K. SERS – a single-molecule and nanoscale tool for bioanalytics. *Chem. Soc. Rev*. **2008**, *37*, 1052–1060.

(10) Maier, S. A. Plasmonic field enhancement and SERS in the effective mode volume

picture. *Opt. Express* **2006**, *14*, 1957–1964.

(11) Maier, S. A. *Plasmonics: fundamentals and applications*; Springer Science & Business Media, 2007.

(12) Gramotnev, D. K.; Bozhevolnyi, S. I. Plasmonics beyond the diffraction limit. *Nat. Photonics* **2010**, *4*, 83.

(13) Schuller, J. A.; Barnard, E. S.; Cai, W.; Jun, Y. C.; White, J. S.; Brongersma, M. L. Plasmonics for extreme light concentration and manipulation. *Nat. Mater.* **2010**, *9*, 193.

(14) Mayer, K. M.; Hafner, J. H. Localized surface plasmon resonance sensors. *Chemical reviews* **2011**, *111*, 3828–3857.

(15) Søndergaard, T.; Bozhevolnyi, S. Slow-plasmon resonant nanostructures: Scattering and field enhancements. *Phys. Rev. B* **2007**, *75*, 073402.

(16) Wei, H.; Xu, H. Hot spots in different metal nanostructures for plasmon-enhanced Raman spectroscopy. *Nanoscale* **2013**, *5*, 10794–10805.

(17) Hamon, C.; Novikov, S. M.; Scarabelli, L.; Solís, D.; Altantzis, T.; Bals, S.; Taboada, J.; Obelleiro, F.; Liz-Marzán L. M. Collective Plasmonic Properties in Few-Layer Gold Nanorod Supercrystals. *ACS Photonics.* **2015**, *2*, 1482–1488.

(18) Yap, F. L.; Thoniyot, P.; Krishnan, S. and Krishnamoorthy, S. Nanoparticle cluster arrays for high-performance SERS through directed self-assembly on flat substrates and on optical fibers. *ACS Nano* **2012***, 6*, 2056–2070.

(19) Tatarkin, D. E.; Yakubovsky, D. I.; Ermolaev, G. A.; Stebunov, Y. V.; Voronov, A. A.; Arsenin, A. V.; Volkov, V. S. and Novikov, S. M. Surface-Enhanced Raman Spectroscopy on Hybrid Graphene/Gold Substrates near the Percolation Threshold. *Nanomaterials* **2020**, *10*, 164.

(20) Moskovits, M. Imaging: Spot the hotspot. *Nature* **2011***, 469*, 307–308.

(21) Polavarapu, L.; La Porta, A.; Novikov, S. M.; Coronado-Puchau, M. and Liz-Marzan, L. M. Pen-on-Paper Approach Toward the Design of Universal Surface Enhanced Raman Scattering Substrates. *Small*, **2014**, *10*, 3065-3071.

(22) Rodal-Cedeira, S.; Montes-García, V.; Polavarapu, L.; Solís, D. M.; Heidari, H.; La Porta, A.; Angiola, M.; Martucci, A.; Taboada, J. M.; Obelleiro, F.; Bals, S.; Perez-Juste, J.; Pastoriza-Santos, I. Plasmonic Au@Pd Nanorods with Boosted Refractive Index Susceptibility and SERS Efficiency: A Multifunctional Platform for Hydrogen Sensing and Monitoring of Catalytic Reactions. *Chem. Mater*. **2016**, *28*, 9169−9180.

(23) Solís, D. M.; Taboada, J. M.; Obelleiro, F. and Liz-Marzán L. M., García de Abajo, F.J. Optimization of Nanoparticle-Based SERS Substrates through Large-Scale Realistic Simulations. *ACS Photonics* **2017**, *4*, 329-337.

(24) Bozhevolnyi, S. I.; Søndergaard, T. General properties of slow-plasmon resonant nanostructures: nano-antennas and resonators. *Opt. Express* **2007**, *15*, 10869–10877.

(25) Søndergaard, T.; Jung, J.; Bozhevolnyi, S. I.; Della Valle, G. Theoretical analysis of gold nano-strip gap plasmon resonators. *New Journal of Physics* **2008**, *10*, 105008.

(26) Jung, J.; Søndergaard, T.; Bozhevolnyi, S. I. Gap plasmon-polariton nanoresonators: Scattering enhancement and launching of surface plasmon polaritons. *Phys. Rev. B* **2009**, *79*, 035401.

(27) Nielsen, M. G.; Gramotnev, D. K.; Pors, A.; Albrektsen, O.; Bozhevolnyi, S. I. Continuous layer gap plasmon resonators. *Opt. Express* **2011**, *19*, 19310–19322.

(28) Baumberg, J. J.; Aizpurua, J.; Mikkelsen, M. H.; Smith, D. R. Extreme nanophotonics from ultrathin metallic gaps. *Nat. Mater.* **2019**, *18*, 668–678.

(29) Gottheim, S.; Zhang, H.; Govorov, A. O.; Halas, N. J. Fractal nanoparticle plasmonics: The Cayley tree. *ACS Nano* **2015**, *9*, 3284–3292.

(30) Wallace, G. Q.; Lagugné-Labarthet, F. Advancements in fractal plasmonics: structures, optical properties, and applications. *Analyst* **2019**, *144*, 13–30.

(31) Huang, X.; Xiao, S.; Ye, D.; Huangfu, J.; Wang, Z.; Ran, L.; Zhou, L. Fractal plasmonic metamaterials for subwavelength imaging. *Opt. Express* **2010**, *18*, 10377–10387.

(32) Zhu, L.-H.; Shao, M.-R.; Peng, R.-W.; Fan, R.-H.; Huang, X.-R.; Wang, M. Broadband absorption and efficiency enhancement of an ultra-thin silicon solar cell with a plasmonic fractal. *Opt. Express* **2013**, *21*, A313–A323.

(33) Aslan, E.; Turkmen, M. Refractive index sensing characteristics of dual resonances in rectangular fractal nano-apertures. *Optical Materials* **2015**, *46*, 423–428.

(34) Fang, J.; Wang, D.; DeVault, C. T.; Chung, T.-F.; Chen, Y. P.; Boltasseva, A.; Shalaev, V. M.; Kildishev, A. V. Enhanced graphene photodetector with fractal metasurface. *Nano Lett.* **2016**, *17*, 57–62.

(35) Beermann, J.; Radko, I. P.; Boltasseva, A.; Bozhevolnyi S. I. Localized field enhancements in fractal shaped periodic metal nanostructures. *Opt. Express* **2007**, *15*, 15234-41.

(36) Radko, I. P.; Volkov, V. S.; Beermann, J.; Evlyukhin, A. B.; Søndergaard, T.; Boltasseva, A.; Bozhevolnyi, S. I. Plasmonic metasurfaces for waveguiding and field enhancement. *Laser & Photon. Rev.* **2009**, *3*, 575–590.

(37) Mandelbrot, B. B. *The fractal geometry of nature*; WH freeman New York, 1983; Vol. 173.

(38) Beermann, J.; Evlyukhin, A.; Boltasseva, A.; Bozhevolnyi, S. I. Nonlinear microscopy of localized field enhancements in fractal shaped periodic metal nanostructures. *JOSA*

B **2008**, *25*, 1585–1592.

(39) Even, C.; Russ, S.; Repain, V.; Pieranski, P.; Sapoval, B. Localizations in fractal drums: an experimental study. *Phys. Rev. Lett.* **1999**, *83*, 726.

(40) Beermann, J.; Novikov, S. M.; Albrektsen, O.; Nielsen, M. G.; Bozhevolnyi, S. I. Surface-enhanced Raman imaging of fractal shaped periodic metal nanostructures. *JOSA B* **2009**, *26*, 2370–2376.

(341) Beermann, J.; Novikov, S. M.; Leosson, K.; Bozhevolnyi, S. I. Surface enhanced Raman microscopy with metal nanoparticle arrays. *Journal of Optics A: Pure and Applied Optics* **2009**, *11*, 075004.

(42) Beermann, J.; Novikov, S. M.; Leosson, K.; Bozhevolnyi, S. I. Surface enhanced Raman imaging: periodic arrays and individual metal nanoparticles. *Opt. Express* **2009**, *17*, 12698–12705.

(43) Nielsen, M. G.; Pors, A.; Albrektsen, O.; Bozhevolnyi, S. I. Efficient absorption of visible radiation by gap plasmon resonators. *Opt. Express* **2012**, *20*, 13311-13319.

(44) Roberts, A. S.; Pors, A.; Albrektsen, O.; Bozhevolnyi, S. I. Subwavelength Plasmonic Color Printing Protected for Ambient Use. *Nano Lett*. **2014**, *14*, 783–787.

(45) Roberts, A. S.; Novikov, S. M.; Yang, Y.; Chen, Y.; Boroviks, S.; Beermann, J.; Mortensen, N. A. and Bozhevolnyi, S. I. Laser Writing of Bright Colors on Near-Percolation Plasmonic Reflector Arrays. *ACS Nano* **2019**, *13*, 71-77.

(46) Pors, A and Bozhevolnyi, S. I. Plasmonic metasurfaces for efficient phase control in reflection, *Opt. Express* **2013**, *21*, 27438-27451.

(47) Lin, K.-Q.; Yi, J.; Zhong, J.-H.; Hu, S.; Liu, B.-J.; Liu, J.-Y.; Zong, C.; Lei, Z.-C.; Wang, X.; Aizpurua, J. Plasmonic Photoluminescence for Recovering Native Chemical Information from Surface-Enhanced Raman Scattering. *Nat. Commun*. **2017**, *8*, 14891.

(48) Ding, S.-Y.; Yi, J.; Li, J.-F.; Ren, B.; Wu, D.-Y.; Panneerselvam, R.; Tian, Z.-Q. Nanostructure-Based Plasmon-Enhanced Raman Spectroscopy for Surface Analysis of Materials. *Nat. Rev. Mater*. **2016,** *1*, 16021.

(49) Itoh, T.; Yoshida, K.; Biju, V.; Kikkawa, Y.; Ishikawa, M.; Ozaki, Y. Second Enhancement in Surface-Enhanced Resonance Raman Scattering Revealed by an Analysis of Anti-Stokes and Stokes Raman Spectra. *Phys. Rev. B: Condens. Matter Mater. Phys*. **2007**, *76*, 085405.

(50) Le Ru, E. C.; Blackie, E.; Meyer, M.; Etchegoin, P. G. Surface Enhanced Raman Scattering Enhancement Factors: A Comprehensive Study. J. *Phys. Chem. C* **2007**, *111*, 13794−13803.

TOC/Abstract Graphic

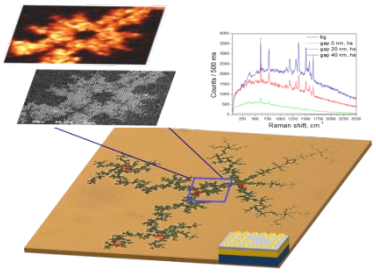

Fractal shaped periodic metal nanostructures atop dielectric-metal substrates for SERS applications
S. M. Novikov, S. Boroviks, A. B. Evlyukhin, D. E. Tatarkin, A. V. Arsenin, V. S. Volkov and S. I. Bozhevolnyi.

Experimentally measured the SERS spectra from the fractal shaped structures on the gold film with a spacer of SiO_2